INTERNATIONAL JOURNAL OF CIRCUITS, SYSTEMS AND SIGNAL PROCESSING
DOI: 10.46300/9106.2023.17.20 Volume 17, 2023

Underwater acoustic positioning for close sources using time division and code division multiplexing

Shingo Yoshizawa[1], Atsushi Wada[1], Hideki Sugimoto[2]
[1]Kitami Institute of Technology, Kitami, Hokkaido, 0908507, Japan
[2]Penta-Ocean Construction Corporation, Tochigi, 329-2746, Japan

Received: September 11, 2022. Revised: February 15, 2023. Accepted: March 4, 2023.
Published: March 29, 2023.

Abstract— Underwater acoustic positioning system (UAPS) is used to know the positions of underwater robots and underwater structures. In ultra-short baseline (USBL) acoustic positioning systems, the three-dimensional position is determined by measuring the time difference of arrival (TDOA). In this paper, we investigate the acoustic positioning system targeting multiple sound sources and propose a simultaneous multi-point measurement method using time division and code division multiplexing (TD-CDM). TD-CDM provides higher position accuracy than code division multiplexing (CDM) and has a much shorter positioning time than time division and multiplexing (TDM). The effectiveness of TD-CDM has been proven by the results of the water tank experiment and simulation.

Keywords— underwater acoustic positioning, time difference of arrival, time division and code division multiplexing, multipath interference

I. Introduction

Underwater acoustic positioning system (UAPS) is used to know the positions of underwater robots and underwater structures, [1]. The positioning methods of UAPS are generally categorized into three types called long baseline (LBL), short baseline (SBL), and ultra-short baseline (USBL). USBL uses a small array of receiver hydrophones and estimates the arrival of angles (AOAs) of a sound source and a distance between a sound source and a receiver element.

The methods of AOA estimation are classified into beamforming, [2], [3], and time difference of arrival (TDOA) measurement, [4], [5]. We have studied the latter. TDOA measurement is suitable for estimating the AOA with a simple array having two receiving elements.

In the TDOA measurement on UAPS, matched filter (MF), [6], generalized cross-correlation with phase transform (GCC-PHAT), [7], and zero-crossing, [8], algorithms have been adopted in the related works. In our previous work, we presented impulse response-based GCC-PHAT (IR-GCC-PHAT) as a countermeasure to multipath interference, [9], [10].

This paper focuses on the acoustic positioning system targeting multiple sound sources. Underwater positioning methods for detecting multiple terminal locations are often, discussed in underwater wireless sensor networks (UASNs), [11], [12], where a distance between terminals and an AOA is collected via communication between acoustic modems. In typical UASNs, the positioning targets are far apart and it takes a long time to get the positions of all terminals. We assume a simultaneous multi-point measurement that the sound sources are densely located, which differs from the method used in UASNs. One of the applications of simultaneous multi-point measurement is to monitor the position and posture of underwater robots and underwater structures.

The simultaneous multi-point measurement has hardly been discussed in the research field of UAPS. As for indoor positioning, the acoustic localization by the use of code division multiplexing (CDM) was reported in [13]. The fundamental idea of CDM is to assign a different spreading code to each sound source. CDM has a shorter positioning time than time division multiplexing (TDM). However, CDM should take into account the interference between sound sources. In underwater acoustics, the strong reflection of acoustic waves occurs on the water's surface, water bottom, and surrounding walls. Those reflections add further interference to degrade the positioning accuracy of CDM.

We propose a simultaneous multi-point measurement method using time division and code division multiplexing (TD-CDM). TD-CDM takes an appropriate trade-off between positioning accuracy and time by adjusting an overlap ratio in sound source sections. In addition, we evaluate positioning accuracy by comparing MF and IR-GCC-PHAT algorithms in the TDOA measurement algorithms. IR-GCC-PHAT shows higher positioning accuracy than MF in a highly reflective environment.

This paper is organized as follows. Section II explains the signal model and TDOA measurement algorithms on the

simultaneous multi-point measurement. Section III presents the three types of multiplexing techniques. Section IV reports the experimental results of acoustic positioning. Section V discusses the proposed and conventional methods from the simulation results. Section VI summarizes our work.

II. Simultaneous Multi-Point Measurement

A. Signal Model

As well as our previous work, [10], we determine a three-dimensional position from two receiving elements and a depth sensor. The vertical position can be accurately measured in centimeters by the depth sensor, [14]. We explain how to measure a distance and an AOA from the two received signals.

Given a sound source index u for the number of sources U, the two received signals $y_1(k)$ and $y_2(k)$ can be modeled by using a transmitted signal $x_u(k)$ and impulse responses $h_{1u}(k)$ and $h_{2u}(k)$ as

$$\begin{aligned} y_1(k) &= \sum_{u=1}^{U}\{h_{1u}(k) * x_u(k)\} + n_1(k) \\ y_2(k) &= \sum_{u=1}^{U}\{h_{2u}(k) * x_u(k)\} + n_2(k), \end{aligned} \tag{1}$$

where k indicates a discrete time index and $*$ shows a convolution operation. $n_1(k)$ and $n_2(k)$ are noise components uncorrelated with the transmitted signal. It is necessary to separate the transmitted signals from the received signals for individual sources. The sound source separation will be discussed in Section III.

If the source separation is ideally performed, the desired signals for the sound source index u can be expressed as

$$\begin{aligned} y_{1u}(k) &= h_1(k) * x_u(k) + n_1(k) \\ y_{2u}(k) &= h_2(k) * x_u(k) + n_2(k). \end{aligned} \tag{2}$$

Since the transmitted signals are used as reference signals on the receiver side as for UAPS, their arrival times can be detected by computing cross-correlation functions. We use the FFT method, [15], for faster computation. The received signals of (2) are modeled in the frequency domain as

$$\begin{aligned} Y_{1u}(l) &= \mathrm{DFT}_N[y_{1u}(k)] = H_{1u}(l)X_u(l) + N_1(l) \\ Y_{2u}(l) &= \mathrm{DFT}_N[y_{2u}(k)] = H_{2u}(l)X_u(l) + N_2(l), \end{aligned} \tag{3}$$

where $\mathrm{DFT}_N[\cdot]$ indicates the discrete Fourier transform for N samples and l denotes a discrete frequency index.

The block diagram of computing a distance and an AOA for each source is illustrated in Fig. 1. The AOA is computed from the TDOA measurement. We compare the MF and IR-GCC-PHAT in the TDOA measurement algorithms.

B. MF

In typical UAPSs, the arrival time of the sound source is measured by computing the cross-correlation function between the transmitted and reference signals. The cross-correlation functions are computed as

$$\begin{aligned} \Phi_{1u}(k) &= \mathrm{IDFT}_N[Y_1(l)X_u^*(l)] \approx h_{1u}(k) \\ \Phi_{2u}(k) &= \mathrm{IDFT}_N[Y_2(l)X_u^*(l)] \approx h_{2u}(k). \end{aligned} \tag{4}$$

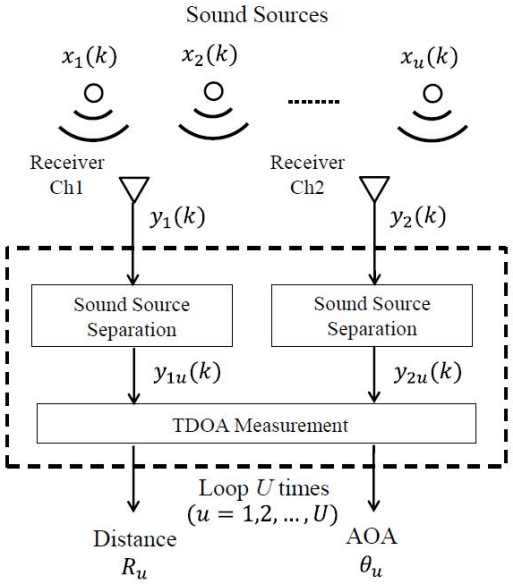

Fig. 1 Computation of a distance and an AOA for each sound source.

The correlation functions of $\Phi_{1u}(k)$ and $\Phi_{2u}(k)$ are approximated by the impulse responses of $h_{1u}(k)$ and $h_{2u}(k)$ for the assumption of $|X(l)| = 1$, $|H_{1u}(l)| \gg |N_1(l)|$, and $|H_2(l)| \gg |N_2(l)|$ as

$$\begin{aligned} \Phi_{1u}(k) &= \mathrm{IDFT}_N[H_{1u}(l)|X_u(l)|^2 + N_1(l)X_u^*(l)] \\ &= \mathrm{IDFT}_N[H_{1u}(l) + N_1(l)X_u^*(l)] \\ &\approx \mathrm{IDFT}_N[H_{1u}(l)] \\ &\approx h_{1u}(k) \\ \Phi_{2u}(k) &\approx h_{2u}(k). \end{aligned} \tag{5}$$

The distance between the sound source and the first receiver element is computed from the arrival time T_u by detecting the highest peak of the correlation function as

$$R_u = c \cdot T_u = c \cdot \underset{k}{\mathrm{argmax}}\, \Phi_{1u}(k)/f_s, \tag{6}$$

where a sound velocity is given by c and a sampling frequency is given by f_s .

In the MF algorithm, the TDOA τ_u is simply obtained by subtracting the arrival times in the two receiver elements as

$$\tau_u = \underset{k}{\mathrm{argmax}}\, |\Phi_{u1}(k)| - \underset{k}{\mathrm{argmax}}\, |\Phi_{u2}(k)|. \tag{7}$$

The AOA θ_u can be computed from the TDOA by

$$\theta_u = \arcsin\left(\frac{c\tau_u}{d}\right), \tag{8}$$

where d denotes an array spacing between receiver elements.

C. IR-GCC-PHAT

The AOA is sensitive to the TDOA because the array spacing is given from a few centimeters to a few dozen centimeters in USBL. The TDOA measurement is strongly influenced by the

reflection of sound waves. In underwater acoustics, there are many reflected waves due to the reflection on the water's surface, bottom, and obstacles, which causes the pseudo-peaks to appear in the correlation function. MF tends to induce large TDOA measurement errors in a highly reflective environment.

IR-GCC-PHAT prevents the false detection caused by the pseudo peaks in the correlation function by taking generalized cross-correlation (GCC) as

$$G_{1u}(l) = \mathrm{DFT}_N[|\Phi_{1u}(k)|]$$
$$G_{2u}(l) = \mathrm{DFT}_N[|\Phi_{2u}(k)|] \quad (9)$$

$$\psi_u(k) = \mathrm{IDFT}_N\left[\frac{G_{1u}(l)G_{2u}^*(l)}{|G_{1u}(l)G_{2u}^*(l)|}\right] \quad (10)$$

$$\tau_u = \underset{k}{\mathrm{argmax}}\, \psi_u(k). \quad (11)$$

The comparison of MF and IR-GCC-PHAT for a single source has been reported in [9].

D. Calculation of Three-Dimensional Position

When the first receiver element is located at the origin of $[0,0,0]$, the location of the sound source $\boldsymbol{p}_u = [x_u, y_u, z_u]$ can be computed from the estimated distance and AOA:

$$x_u = R_u\cos\theta_u$$
$$y_u = R_u\cos\phi_u$$
$$z_u = D_u$$
$$\cos\phi_u = \sqrt{1 - \cos^2\theta_u - \left(\frac{D_u}{R_u}\right)^2}, \quad (12)$$

where D_u denotes the vertical position measured by a depth sensor. This localization is carried out by a single TDOA, which obtains a higher position accuracy than that of multiple TDOAs, [14].

III. Multiplexing Techniques

The sound source separation (conversion from (1) to (2)) is necessary for the simultaneous multi-point measurement. Multiplexing is a reasonable idea where the sound sources are multiplexed and de-multiplexed in time or code domains. We compare TDM, CDM, and TD-CDM in multiplexing techniques.

A. TDM

TDM prepares individual positioning sections for all sound sources. The timing chart of TDM for U=3 is illustrated in Fig. 2. In the transmitted signals of $x_1(k)$, $x_2(k)$, and $x_3(k)$, their timings of transmitting sound sources are separated by the interval of N. We set the length of the sound source to $N/2$ samples. As shown in the received signal of $y_1(k)$, TDM does not induce interference between sound sources as long as the positioning interval is designed to be longer than the arrival time.

The source separation by TDM is simple. However, it takes a long time to complete positioning for all sources, where the total positioning time becomes UN samples. TDM is not suitable for monitoring the position and posture of underwater robots and underwater structures because the positioning time should be as short as possible.

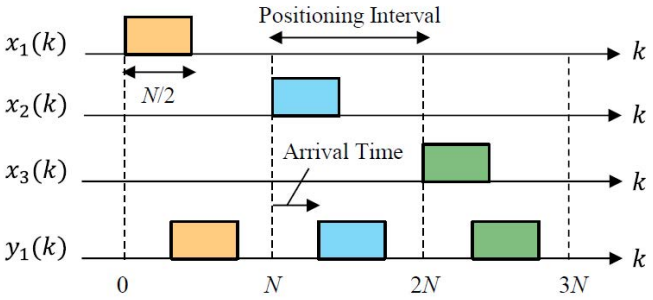

Fig. 2 Timing chart of TDM.

B. CDM

As reported in [13], the use of CDM is effective in terms of shortening the positioning time. The timing chart of CDM is shown in Fig. 3. All sounds are simultaneously transmitted and their source locations are identified by individual reference signals. The total positioning time is N.

The source separation by CDM can be performed in the same way explained in Section II.B. We express the received signal of $y_1(k)$ for U=3 in the frequency domain as

$$Y_1(l) = H_{11}(l)X_1(l) + H_{12}(l)X_2(l) + H_{13}(l)X_3(l) + N_1(l) \quad (13)$$

We compute the cross-correlation function for the first sound source by the following equations:

$$Y_1(l)X_1^*(l) = H_{11}(l)X_1(l)X_1^*(l) + H_{12}(l)X_2(l)X_1^*(l) + H_{13}(l)X_3(l)X_1^*(l) + N_1(l)X_1^*(l) \quad (14)$$

$$\Phi_{11}(k) = \mathrm{IDFT}_N[Y_1(l)X_1^*(l)] \approx h_{11}(k) + n_1'(k). \quad (15)$$

When the transmitted signals are uncorrelated from each other, the components of $H_{12}(l)X_2(l)X_1^*(l)$ and $H_{13}(l)X_3(l)X_1^*(l)$ are whitened after the IDFT operation. The peak detection in (15) is available as far as the noise level of $n_1'(k)$ is low.

The drawback of CDM is increased interference, depending on the number of sources. We should take into account the interference caused by acoustic wave reflection. As reported in Section IV, CDM has large positioning errors in a highly reflective environment. The simultaneous multi-point measurement by CDM is not sufficient in terms of positioning accuracy.

C. TD-CDM

We propose the simultaneous multi-point measurement by TD-CDM, where the timing chart of TD-CDM is illustrated in Fig. 4. The transmit timing for each source is shifted by the overlap length. The DFT timing in (4) is also shifted according to the overlap length.

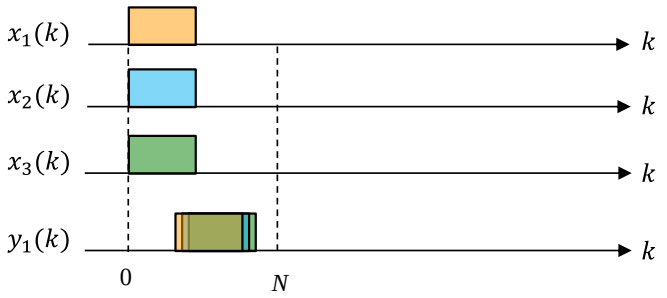

Figure 3. Timing chart of CDM.

When the overlap ratio is defined by L ($0 \leq L \leq 1$), the total positioning time becomes $(U-1)(1-L)N/2+N$. The overlap length is given by $LN/2$. The interference between sound sources can be mitigated by decreasing the value of L.TD-CDM can take an appropriate trade-off between positioning time and accuracy.

The case of L=1 corresponds to CDM. The positioning time for L=0 becomes $(U+1)N/2$, which is different from TDM. The interference between adjoined sources might occur depending on their arrival times in the case of L=0.

We investigate how small the overlap ratio can be while maintaining positioning accuracy, where the results of our experiment and simulation are reported in Sections IV and V.

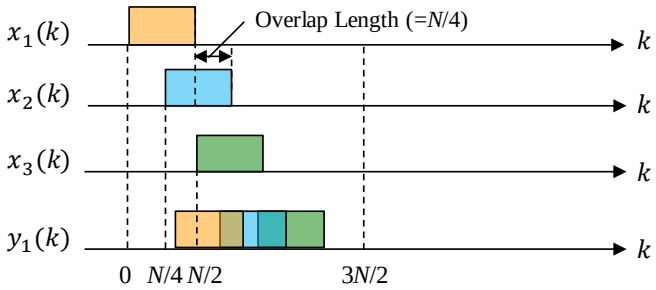

Figure 4. Timing chart of TD-CDM (for case of L=0.5).

IV. Experiment

A. Experimental Conditions

We conducted the underwater acoustic positioning experiment at a large water tank in the Fukushima Robot Test Field, in Fukushima, Japan in December 2021. The size of the water tank is 12 m in width, 30 m in depth, and 6.87 m in height.

Fig. 5 shows the locations of the sound sources and the receiver elements on the x-y graph. The coordinates of the first and second receiver elements are $[6, 5, 5.87]$ and $[5.7, 5, 5.87]$, respectively. The 15 sound sources are arranged horizontally or vertically at intervals of 0.3 m. The horizontal array sound sources are located from $[3, 5, 2.87]$ to $[7.2, 5, 2.87]$. The vertical array sound sources are located from $[2, 15, 1.9]$ to $[2, 15, 6.1]$. The installation of the horizontal and vertical arrays is shown in Fig. 6.

We use pseudo-noise signals that are generated by a sequence of PN codes for the 15 sound sources. Their signal

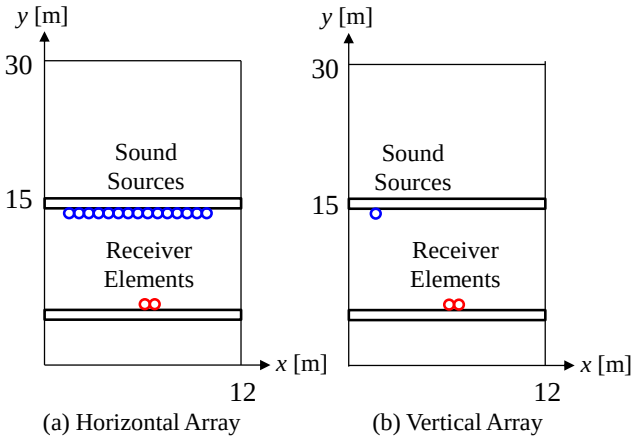

Figure 5. Locations of sound sources and receiver elements.

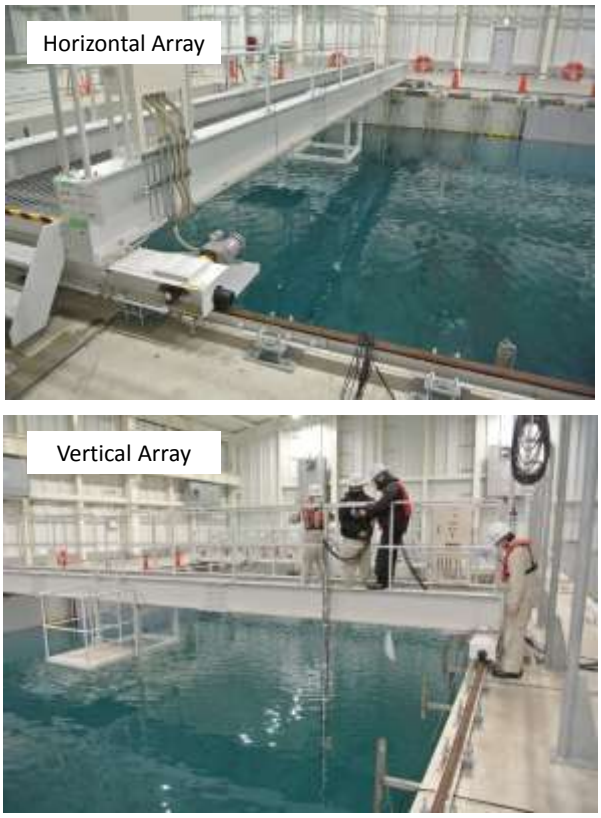

Figure 6. Installation of the horizontal and vertical arrays.

length is 16,384 samples and corresponds to 65.5 ms for a sampling frequency of 250 kHz. The signal frequency band is from 12 kHz to 32 kHz. The parameters of U, and N correspond to 15 and 32,768. The overlap ratio L is set to 0, 0.2, 0.4, 0.6, 0.8, and 1 for each test. The conventional method (CDM) corresponds to L=1. The proposed method (TD-CDM) ranges from L=0 to L=0.8. We compare MF and IR-GCC-PHAT to evaluate positioning accuracy in the TDOA measurement algorithms. The average signal-to-noise ratio (SNR) was 33 dB.

B. Experimental Results

The vertical position for each source on the z-axis is

Table 1. Experimental results.

(a) Horizontal Array

Average Error [m]	TD-CDM					CDM
Overlap Ratio	0	0.2	0.4	0.6	0.8	1
MF	7.11	4.95	5.71	6.90	9.53	11.34
IR-GCC-PHAT	0.27	0.29	0.33	1.77	5.69	7.93

(b) Vertical Array

Average Error [m]	TD-CDM					CDM
Overlap Ratio	0	0.2	0.4	0.6	0.8	1
MF	1.33	3.16	2.31	4.19	8.85	15.37
IR-GCC-PHAT	0.22	0.31	0.22	0.31	1.65	11.27

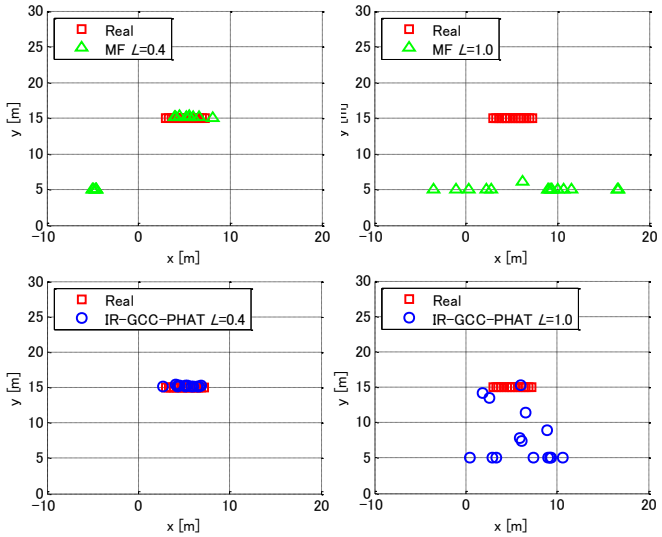

Figure 7. Real and measured positions in horizontal array.

measured by the depth sensor. We compare the real position with the measured position on the x-y coordinates. The two-dimensional positioning error for each source is given by

$$E_u = \sqrt{(\overline{x_u} - x_u)^2 + (\overline{y_u} - y_u)^2}, \tag{15}$$

where $\overline{x_u}$ and $\overline{y_u}$ are the coordinates of a real position with a u-th source. The average positioning error for all sources is evaluated.

Table 1 shows the results of average positioning errors for the horizontal and vertical arrays. When we compare the results in MF and IR-GCC-PHAT, MF is sensitive to the acoustic reflection and its positioning performance is insufficient for a large number of sources. IR-GCC-PHAT is mandatory for the simultaneous multi-point measurement. CDM (L=1) has a large error with an average error of 7 m or more. On the other hand, TD-CDM can decrease a positioning error by taking an appropriate overlap ratio. The appropriate overlap ratios become 0.4 and 0.6 for the horizontal and vertical arrays when we set the allowable error to less than 0.5 m. We confirmed that the simultaneous multi-point measurement is possible even in a

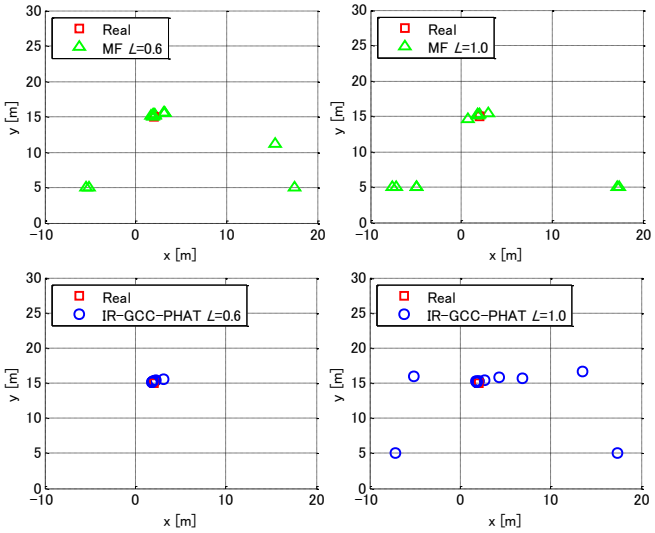

Figure 8. Real and measured positions in vertical array.

highly reflective environment by adjusting the overlap ratio.

Fig. 7 shows the real and measured positions in the horizontal array. The case of MF with L=0.4 has large positioning errors for several sources (plotted at around $[-5, 5]$). It comes from the AOA estimation error where the TDOA measurement by MF is strongly affected by acoustic reflections (see, [9], for the details).

Fig. 8 shows the real and measured positions in the vertical array. All sources are drawn at the same position on the x-y graph when there is no positioning error. The acoustic positioning of the vertical array gives slightly better than that of the horizontal array.

V. Discussion

A. Simulation Results under Various Conditions

We investigate the simultaneous multipoint measurement under various conditions in simulation. We use a sound wave propagation simulator as well as our previous works, [9], [10]. The impulse response is obtained by determining the size of acoustic field, the reflectance ratios, and the positions of sound

Table 2. Simulation results with a 30-dB SNR under reflective environment.

(a) Horizontal Array

Average Error [m]	TD-CDM					CDM
Overlap Ratio	0	0.2	0.4	0.6	0.8	1
MF	6.83	5.94	6.08	7.72	9..27	14.37
IR-GCC-PHAT	0.20	0.18	0.29	0.31	1.06	7.62

(b) Vertical Array

Average Error [m]	TD-CDM					CDM
Overlap Ratio	0	0.2	0.4	0.6	0.8	1
MF	6.46	2.87	6.99	4.69	8.96	9.97
IR-GCC-PHAT	0.15	0.15	0.24	0.33	0.40	4.80

Table 3. Simulation results with a 30-dB SNR under non-reflective environment.

(a) Horizontal Array

Average Error [m]	TD-CDM					CDM
Overlap Ratio	0	0.2	0.4	0.6	0.8	1
MF	0.16	0.16	0.16	0.16	0.16	0.23
IR-GCC-PHAT	0.12	0.12	0.13	0.13	0.16	0.23

(b) Vertical Array

Average Error [m]	TD-CDM					CDM
Overlap Ratio	0	0.2	0.4	0.6	0.8	1
MF	0.11	0.11	0.11	0.11	0.11	0.13
IR-GCC-PHAT	0.11	0.11	0.11	0.10	0.11	0.11

Table 4. Simulation results with a 0-dB SNR under non-reflective environment.

(a) Horizontal Array

Average Error [m]	TD-CDM					CDM
Overlap Ratio	0	0.2	0.4	0.6	0.8	1
MF	0.16	0.16	0.16	0.16	0.16	4.19
IR-GCC-PHAT	0.13	0.13	0.14	0.14	0.28	2.55

(b) Vertical Array

Average Error [m]	TD-CDM					CDM
Overlap Ratio	0	0.2	0.4	0.6	0.8	1
MF	0.11	0.11	0.11	0.12	0.11	2.49
IR-GCC-PHAT	0.11	0.11	0.11	0.10	0.11	0.42

sources and receiver elements. The additive white Gaussian noise (AWGN) is added to a transmit signal.

Table 2 shows the results of average positioning errors with a 30-dB SNR under a reflective environment. In the reflective environment, we set the reflectance ratios to 1 for the water surface and 0.7 for the water bottom and surrounding walls. This condition reproduces the water tank at the time of the experiment. The allowable overlap ratios (the average positioning error is less than 0.5 m) in IR-GCC-PHAT are 0.6 and 0.8 for the horizontal and vertical arrays. Although the simulation shows better results than the experiment, trends in the overlap ratios are well aligned.

Table 3 shows the results of average positioning errors with a 30-dB SNR under a non-reflective environment. This condition gives sufficient positioning accuracy regardless of multiplexing techniques and TDOA measurement algorithms. CDM would be most effective in terms of positioning time.

Table 4 shows the results of average positioning errors with a 0-dB SNR under a non-reflective environment. There is not much difference in positioning accuracy between MF and IR-GCC-PHAT. The positioning errors of CDM are larger than those of TD-CDM, unlike the case of Table 3.

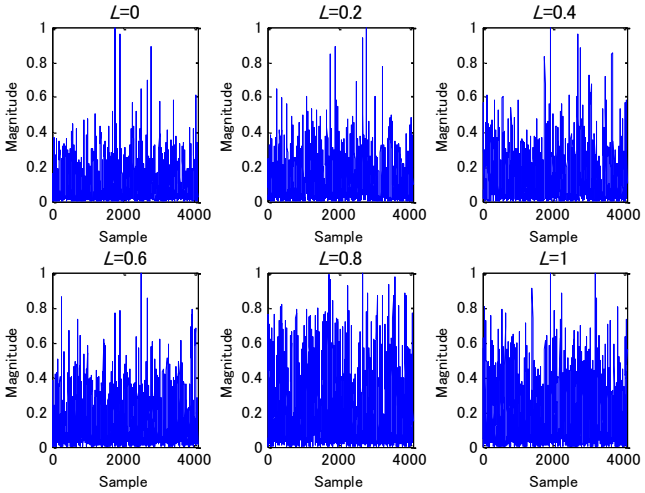

(a) 30-dB SNR under Reflective Environment

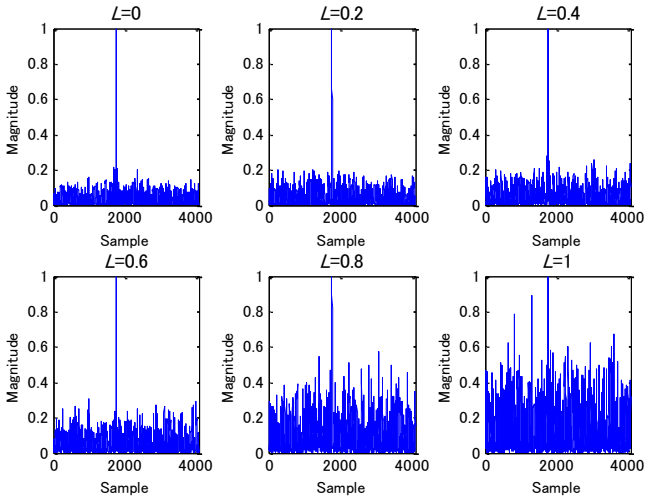

(b) 0-dB SNR under Non-Reflective Environment

Figure 9. Cross correlation functions for 11-th source in horizontal array.

B. Cross-correlation Functions in Simultaneous Multi-point Measurement.

Fig. 9(a) shows the cross-correlation functions $\Phi_{1u}(k)$ for the 11-th source in a horizontal array. Fig.9(a) investigates the high SNR condition under a highly reflective environment. Although the background noise level is low, the pseudo peaks caused by acoustic reflections are observed. IR-GCC-PHAT is more robust with those pseudo peaks than MF, [9]. It is difficult to detect a correct AOA even for IR-GCC-PHAT for the cases of L=0.8 and L=1 the interference between sources is heavily affected.

Fig. 9(b) investigates the low SNR condition under a non-reflective environment. There is no pseudo peak for the cases from L=0 to L=0.8. It enables the detection of a correct AOA regardless of TDOA measurement algorithms. The pseudo peaks are observed for the case of L=1 because the interference between sources is large.

The interference between sound sources and the interference caused by noise and acoustic reflection can be collectively represented by $n_1'(k)$ in (15). When there is only interference between sound sources, CDM provides satisfactory positioning accuracy. However, CDM degrades positioning accuracy in realistic environments under low SNR or highly reflective conditions. TD-CDM can mitigate interference between sound sources to tolerate interference from noise and acoustic reflections and maintain short positioning time.

VI. Conclusion

This paper has presented the simultaneous multi-point measurement method using TD-CDM. We explained the signal model on the simultaneous multi-point measurement, where the source separation is mandatory to detect a distance and an AOA for every source. We compared TDM, CDM, and TD-CDM as multiplexing techniques and asserted that TD-CDM is effective from both sides of positioning accuracy and time. The effectiveness of TD-CDM was proven by the experimental and simulation results.

In our future work, we will investigate acoustic positioning systems when sound sources are moving. The countermeasure for Doppler shifts would be required for the above situation.

Acknowledgment

The authors would like to thank Mr. Satoshi Yuasa for his support and assistance with this project. This work was supported by JSPS KAKENHI Grant Number 20K04477.

References

[1] L. Paull, S. Saeedi, M. Seto, and H. Li, "AUV navigation and localization: a review," IEEE Journal of Oceanic Engineering, vol. 39, no. 1, pp. 131-149, Jan. 2014.

[2] M. Jian, A. C. Kot, and M. H. Er, "DOA estimation of speech source with microphone arrays," IEEE International Symposium on Circuits and Systems (ISCAS), pp. 293-296, May 1998.

[3] J. Zhuang, T. Tan, D. Chen, and J. Kang, "DOA tracking via signal subspace projector update," IEEE International Conference on Acoustics, Speech and Signal Processing (ICASSP), pp. 4905-4909, May 2020.

[4] H. Kang, M. Graczyk, and J. Skoglund, "On pre-filtering strategies for the GCC-PHAT algorithm," IEEE International Workshop on Acoustic Signal Enhancement (IWAENC), pp. 1-5, Sep. 2016.

[5] Z. Q. Wang, X. Zhang, and D. Wang, "Robust TDOA estimation based on time frequency masking and deep neural networks," 19th Annual Conference of the International Speech Communication Association (Interspeech 2018), pp. 322-326, Aug. 2018.

[6] B. Kouzoundjian, F. Beaubois, S. Reboul, and J. B. Choquel, and J. Noyer, "A TDOA underwater localization approach for shallow water environment," MTS/IEEE OCEANS 2017 - Aberdeen, pp. 1-4, June 2017.

[7] J. Choi, J. Park, Y. Lee, J. Jung, and H. Choi, "Robust directional angle estimation of underwater acoustic sources using a marine vehicle," MDPI Sensors, vol. 18, issue 9, pp. 1-14, Sep. 2018.

[8] J. F. Valente and J. C. Alves, "Real-time TDOA measurements of an underwater acoustic source," MTS/IEEE OCEANS 2016 - Monterey, pp. 1-7, Sep. 2016.

[9] S. Yoshizawa, "Underwater acoustic localization based on IR-GCC-PHAT in reverberant environments," International Journal of Circuits, Systems and Signal Processing, vol. 15, pp.164-171, Mar. 2021.

[10] S. Yoshizawa, "Impulse response shortening in TDOA algorithm for underwater acoustic localization," International Journal of Circuits, Systems and Signal Processing, vol. 15, pp.1624-1631, Nov. 2021.

[11] M. T. Isik and O. B. Akan, "A three dimensional localization algorithm for underwater acoustic sensor networks," IEEE Transactions on Wireless Communications, vol. 8, no. 9, pp. 4457-4463, Sep. 2009.

[12] I. Ullah, J. Chen, X. Su, C. Esposito and C. Choi, "Localization and detection of targets in underwater wireless sensor using distance and angle based algorithms," IEEE Access, vol. 7, pp. 45693-45704, Apr. 2019.

[13] F. Seco, A. R. Jiménez and F. Zampella, "Fine-grained acoustic positioning with compensation of CDMA interference," IEEE International Conference on Industrial Technology (ICIT), pp. 3418-3423, Mar. 2015.

[14] A. Wada, S. Yoshizawa, "Transmission of depth data by pulse position modulation for underwater acoustic positioning systems," International Journal of Circuits, Systems and Signal Processing, vol. 16 pp.999-1006, May 2022.

[15] W. H. Press, B. P. Flannery, S. A. Teukolsky, W. T. Vetterling, "Numerical Recipes in FORTRAN: The Art of Scientific Computing," England Cambridge University Press, pp. 538-539, 1992.

Contribution of individual authors to the creation of a scientific article (ghostwriting policy)

We confirm that all Authors equally contributed in the present research, at all stages from the formulation of the problem to the final findings and solution.

Sources of funding for research presented in a scientific article or scientific article itself

This work was supported by JSPS KAKENHI Grant Number 20K04477.

Conflict of Interest

The authors have no conflict of interest to declare that is relevant to the content of this article.